

SYNCHROTRON MAGNETIC FIELDS FROM RAYLEIGH-TAYLOR INSTABILITY IN SUPERNOVAE

PAUL C. DUFFELL AND DANIEL KASEN

Astronomy Department and Theoretical Astrophysics Center, University of California, Berkeley, CA 94720
Draft version October 6, 2018

ABSTRACT

Synchrotron emission from a supernova necessitates a magnetic field, but it is unknown how strong the relevant magnetic fields are, and what mechanism generates them. In this study, we perform high-resolution numerical gas dynamics calculations to determine the growth of turbulence due to Rayleigh-Taylor instability, and the resulting kinetic energy in turbulent fluctuations, to infer the strength of magnetic fields amplified by this turbulence. We find that Rayleigh-Taylor instability can produce turbulent fluctuations strong enough to amplify magnetic fields to a few percent of equipartition with the thermal energy. This turbulence stays concentrated near the reverse shock, but averaging this magnetic energy throughout the shocked region (weighting by emissivity) sets the magnetic fields at a minimum of 0.3 percent of equipartition. This suggests a minimum effective magnetic field strength ($\epsilon_B > 0.003$) which should be present in all interacting supernovae.

Subject headings: hydrodynamics — shock waves — instabilities — supernovae: general — ISM: jets and outflows

1. INTRODUCTION

The interaction of the ejecta from a supernova explosion with a surrounding circumstellar medium (CSM) can give rise to synchrotron radiation at radio wavelengths. Radio observations of core collapse supernovae (SNe) have been used to constrain the density and structure of the CSM, with implications for the presupernova evolution and mass loss history of massive stars (e.g., Chevalier & Fransson 2006; Patat et al. 2007). Radio non-detections in Type Ia SNe have been used to place some of the strongest constraints on the progenitor system. Upper limits from deep radio images set bounds on the CSM density from the stellar winds that are expected from certain binary channels (Soderberg et al. 2012; Horesh et al. 2012; Chomiuk et al. 2012, 2015).

Perhaps the largest current uncertainty in physically interpreting the radio emission from interacting SNe is the strength of the magnetic field in interaction region. Essentially all synchrotron modeling to date assumes that the field strength can be characterized by a constant parameter ϵ_B , the ratio of magnetic to thermal energy in the flow. The value of ϵ_B is not well-constrained by theory, as it is unclear what mechanism is responsible for the field’s amplification in supernova shocks. Observation can only set broad limits, as the value of ϵ_B is degenerate with other properties of the flow. The large uncertainty on ϵ_B makes it difficult to make strong inferences from radio non-detections. If there is no minimum “floor” on ϵ_B , then some outflows could have arbitrary small magnetic field, and hence be undetectable in the radio, even if the CSM density is high.

Theoretical constraints on ϵ_B are difficult to make, in part because the underlying cause of the magnetic fields is uncertain. If the magnetic field strength, B , in the supernova is inherited from the progenitor, it will drop quickly as the flow expands via flux freezing: $B \sim B_0(R(t)/R_0)^{-2}$, where B_0 is the surface magnetic field of the progenitor, $R(t)$ is the shock radius, and R_0

is the progenitor size. Assuming a solar-like progenitor with ~ 1 Gauss magnetic field, CSM density of $\rho \sim A/r^2$ with $A = 5 \times 10^{11}$ g/cm and ejecta velocity of 10^9 cm/s, this gives a meager $\epsilon_B \sim B^2/(\rho_{\text{CSM}}v^2) \sim 10^{-8}(R/R_0)^{-2}$, where at typical times of observation, $t \sim 1$ day, the radius $R = vt \gg R_0$. On the other hand, plasma instabilities such as Weibel instability (Gruzinov & Waxman 1999; Medvedev & Loeb 1999) have been shown to amplify magnetic fields to $\epsilon_B \sim 10\%$ in the context of relativistic jets (Nishikawa et al. 2003; Spitkovsky 2008). However, it is expected that this field should only be present within a few plasma skin depths of the forward shock, resulting in a negligible emitting volume for non-relativistic SN interactions.

While the prospects of calculating an ϵ_B from theory have previously seemed remote, we argue here that a robust minimal value can be estimated from straightforward hydrodynamical calculations. Interacting SNe are turbulent due to Rayleigh-Taylor (RT) instability, so a magnetic field in the flow is necessarily set by small scale turbulent dynamo. We will show numerically that a minimal floor to ϵ_B is set by this process, even if all other processes (e.g. Weibel instability) fail to generate significant magnetic fields.

Amplification of magnetic fields by RT was first studied by Jun et al. (1995) in two and three-dimensions with magnetic fields using local calculations. Jun & Norman (1996) demonstrated in the supernova context (in 2D) that RT could cause these fields to align with turbulent structures, affecting polarization of synchrotron emission. Kane et al. (2000) studied the difference between 2D and 3D, but still in a local sense (looking at single-mode perturbations). That study found that the growth of RT is 30 – 35% stronger in 3D than in 2D. Magnetic amplification due to RT and small-scale turbulent dynamo has also been studied in the relativistic case, in the context of gamma ray bursts (Duffell & MacFadyen 2013, 2014).

Studying the entire process self-consistently in a global calculation is computationally demanding. First, a

proper treatment of MHD turbulence necessitates a 3D calculation. Secondly, capturing small-scale turbulent dynamo in MHD turbulence requires high resolution; at least 256 zones across the largest-scale eddies (Zrake & MacFadyen 2013). This is a known issue, for example, in simulations of merging neutron stars, in which small-scale turbulent dynamo is expected to amplify magnetic fields up to magnetar-levels (Zrake & MacFadyen 2013; Giacomazzo et al. 2015). Global simulations, however, have yet to observe this dramatic amplification (but they have come close; see Kiuchi et al. (2015)).

Rather than attempt a full 3D MHD study which resolves the dynamo, we restrict ourselves to modest 2D hydrodynamics calculations, to determine the amplitude of turbulent fluctuations in the saturated state. We then use this to infer the strength of the magnetic fields as predicted by dynamo theory, and the consequences for the radio emission from SNe. Although a full 3D calculation would be more accurate in many ways (for example, the 2D solution will not have the correct kinetic power spectrum), the 2D calculation will capture the strength of the driving field to order-of-magnitude (as shown by previous studies comparing 2D and 3D RT, e.g. Kane et al. 2000), and this large-scale driving field is what sets the turbulent kinetic energy.

2. NUMERICAL SET-UP

The numerical calculations performed in this study are very similar to those performed by Chevalier et al. (1992), who studied RT instability in interacting SNe. We focus on measuring the kinetic energy density of turbulent fluctuations and mapping this to a magnetic field strength.

Our numerical calculations integrate the equations of two-dimensional (2D) axisymmetric hydrodynamics

$$\partial_t(\rho) + \nabla \cdot (\rho \vec{v}) = 0, \quad (1)$$

$$\partial_t(\rho v_r) + \nabla \cdot (\rho v_r \vec{v} + P \hat{r}) = (2P + \rho v_\theta^2)/r, \quad (2)$$

$$\partial_t(r \rho v_\theta) + \nabla \cdot (r \rho v_\theta \vec{v} + P \hat{\theta}) = P c \cot \theta, \quad (3)$$

$$\partial_t\left(\frac{1}{2}\rho v^2 + \epsilon\right) + \nabla \cdot \left(\left(\frac{1}{2}\rho v^2 + \epsilon + P\right)\vec{v}\right) = 0, \quad (4)$$

where ρ is density, P is pressure, ϵ is the internal energy density, and \vec{v} is the velocity. The equation of state is assumed to be gas pressure dominated: $\epsilon = \frac{3}{2}P$. This is appropriate for interaction with a sufficiently low-density CSM, for which the timescale for the shocked gas to radiate is much longer than the dynamical timescale. A few additional runs were performed with variable adiabatic index, to determine the dependence of the results on the equation of state.

Numerical calculations are carried out using the JET code (Duffell & MacFadyen 2011, 2013), a moving mesh technique that is effectively Lagrangian due to the radial motion of computational zones. The initial conditions at the start time t_0 adopt a power-law profile for both the ejecta density, ρ_{ej} , and the CSM density, ρ_{CSM} ,

$$\rho_{\text{ej}}(r, t_0) = \left(\frac{r}{gt_0}\right)^{-n} t_0^{-3}, \quad (5)$$

$$\rho_{\text{CSM}}(r, t_0) = qr^{-s}, \quad (6)$$

where g and q are constants that set the density scales. For the present study, we choose $n = 7$, $s = 2$. In a similar study, Chevalier et al. (1992) use power-law profiles for the ejecta and CSM structures, but initialized the contact region with the self-similar solutions of Chevalier (1982). In contrast, this study allows the ejecta and CSM to collide and evolve to the self-similar structure. We find that RT instability sets in before the self-similar Chevalier solution has had time to emerge.

Rather than initializing the contact interface between the ejecta and CSM as a step function, it is numerically advantageous to start with a smooth initial condition

$$\rho_{\text{tot}}(r, t_0) = \rho_{\text{ej}}(r, t_0) + \rho_{\text{CSM}}(r, t_0). \quad (7)$$

This initial condition is asymptotically identical to Chevalier's (for both $r \rightarrow 0$ and $r \rightarrow \infty$), and so at late times in 1D it is guaranteed to approach the same self-similar solution.

Additionally, a seed perturbation is introduced, assuming some ‘‘clumpiness’’ to the ejecta and CSM

$$\rho(r, t_0) = \rho_{\text{tot}}(r, t_0)e^{\delta(\vec{r})}, \quad (8)$$

where the fluctuations $\delta(\vec{r})$ are given by

$$\delta(\vec{r}) = \delta_0 \sin(l\theta) \sin(l \ln(r)), \quad (9)$$

with an angular wavenumber l (where $l = 50$ in this study), and a magnitude δ_0 . The ejecta is assumed to be cold, ballistic, and expanding homologously, with a velocity profile

$$v(r, t_0) = \begin{cases} r/t_0 & r < R_0(t_0) \\ 0 & r > R_0(t_0) \end{cases} \quad (10)$$

where $R_0(t) = (qg^n)^{\frac{1}{n-s}} t^{\frac{n-3}{n-s}}$ is the initial contact interface. However, again it is numerically convenient to adopt smooth initial conditions, and therefore we initialize the velocity as

$$v(r, t_0) = (r/t_0) \frac{\rho_{\text{ej}}(r, t_0)}{\rho_{\text{tot}}(r, t_0)}. \quad (11)$$

Again, as this velocity profile is asymptotically identical to Chevalier's at large and small radii, it approaches an identical solution at late times, after the forward and reverse shocks have swept up a sufficient amount of mass.

Additionally, a passive scalar is initialized in the flow, to differentiate ejecta from CSM, and in principle measure the mixing of the two:

$$X(r, \theta, 0) = \begin{cases} 0 & r < R_0(t_0) \\ 1 & r > R_0(t_0) \end{cases} \quad (12)$$

Note that this passive scalar is initialized as a discontinuous function (as opposed to the initial density and velocity) so that values of X that deviate from 1 or 0 are entirely due to mixing. This makes it possible to precisely track which regions of the solution are mixed.

These initial data are then evolved for seven orders of magnitude in time, until $t = 10^7 t_0$. This ensures that the RT instability has reached a saturated, statistically self-similar state (Figure 1).

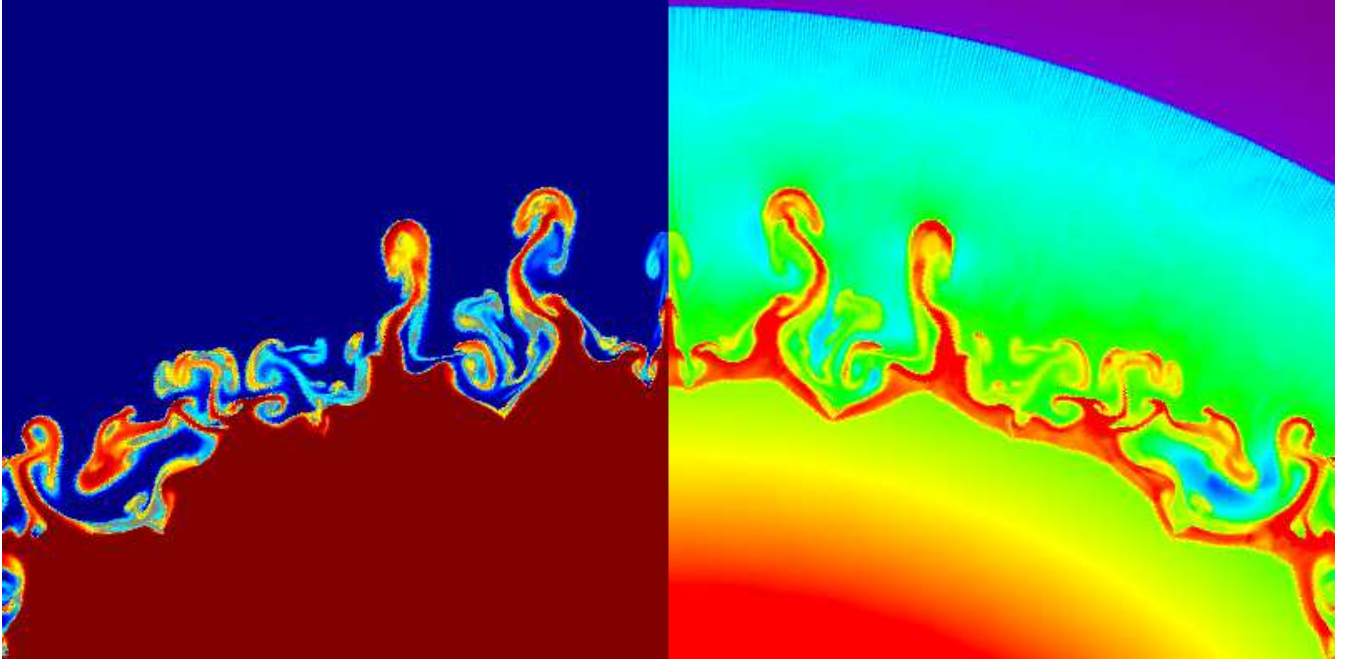


FIG. 1.— Rayleigh-Taylor instability in the case with very small seed density fluctuations $\delta_0 = 0.01$ (compare Figure 6 and 7 of Chevalier et al. (1992)). The left side plots the passive scalar X (ranging between 0 and 1, with 0 for pure ejecta and 1 for pure CSM). The right side plots the logarithm of density (with dimensions scaled out, and $\ln(\rho)$ ranging from 1 to 4).

2.1. Turbulence Measurements and Magnetic Field Amplification

RT instabilities in the interaction region drive turbulent fluctuations that will amplify magnetic fields. We quantify the magnitude of turbulent fluctuations by measuring the amount of kinetic energy in a spherical shell, then subtracting off the part attributed to bulk motion. The total hydrodynamical energy density is a combination of bulk kinetic energy, turbulent kinetic energy, and thermal energy:

$$U_{\text{tot}} = \frac{1}{2}\rho \langle v \rangle^2 + U_{\text{turb}} + P/(\gamma - 1), \quad (13)$$

where $\gamma = 5/3$ is the adiabatic index. The bulk velocity $\langle v \rangle$ is calculated by dividing the spherical shell's momentum by its mass. Pressure and density are evaluated using a simple volume average over the shell. Since all other quantities (including total energy) are known for a given spherical shell, U_{turb} can be found by solving this equation. Then the turbulent energy fraction $\epsilon_{\text{turb}} = U_{\text{turb}}/U_{\text{thermal}}$ can be readily calculated

$$\epsilon_{\text{turb}} = \frac{U_{\text{tot}} - \frac{1}{2}\rho \langle v \rangle^2 - P/(\gamma - 1)}{P/(\gamma - 1)}. \quad (14)$$

The quantity ϵ_{turb} is a measurement of turbulent kinetic energy. Here we argue that $\epsilon_{\text{turb}} \sim \epsilon_B$, i.e. that magnetic fields can be quickly amplified by small scale turbulent dynamo up to rough equipartition with the turbulent fluctuations, regardless of the initial seed field.

Equipartition is established by turbulent dynamo processes, which are known to be present in low-viscosity conducting fluids with high magnetic Prandtl number and a persistent injection of turbulent kinetic energy. Initially, kinematic small-scale turbulent dynamo drives exponential growth of any weak pre-existing magnetic

field at a rate comparable to the turnover time of smallest eddies (Kazantsev 1968; Moffatt 1978). This rate is extremely fast compared to outer-scale eddy turn-over times (in the high Reynolds number limit, this process is effectively instantaneous, which is why it is independent of the initial magnetic field strength).

The kinematic process terminates when the energy in viscous scale magnetic fluctuations balances kinetic energy of viscous scale eddies. Magnetic field amplification then continues via nonlinear small-scale dynamo process (Schekochihin et al. 2004). During the nonlinear phase, the magnetic energy grows linearly with time, as magnetic fluctuations move to progressively larger scales. The nonlinear phase terminates when magnetic fluctuations exist in scale-by-scale equipartition up to the outer scale of the RT-inspired turbulence.

Numerical calculations in the non-relativistic (Haugen et al. 2003; Beresnyak 2012) and relativistic (Zrake & MacFadyen 2013) cases indicate that in the limit of large Reynolds number, non-linear small-scale turbulent dynamo saturates universally after several large-scale turnover times. Therefore, if magnetic fields and 3D resolution of sufficient turbulent sub-scales were included in our calculations, these magnetic fields should quickly end up in kinetic equipartition with turbulent fluctuations. “Equipartition” here means that the ratio of kinetic to magnetic energy $\epsilon_{\text{turb}}/\epsilon_B$ is of order unity. The aforementioned numerical studies have reported end-state turbulent dynamo saturation with magnetic energy at between 30% and 60% of the turbulent kinetic energy density. Therefore, assuming the largest eddies turn over several times during the evolution, $\epsilon_B \approx 0.3 \epsilon_{\text{turb}}$ at the very least.

3. RESULTS

Figure 1 shows fully-developed turbulence after the flow has expanded by five orders of magnitude (here the

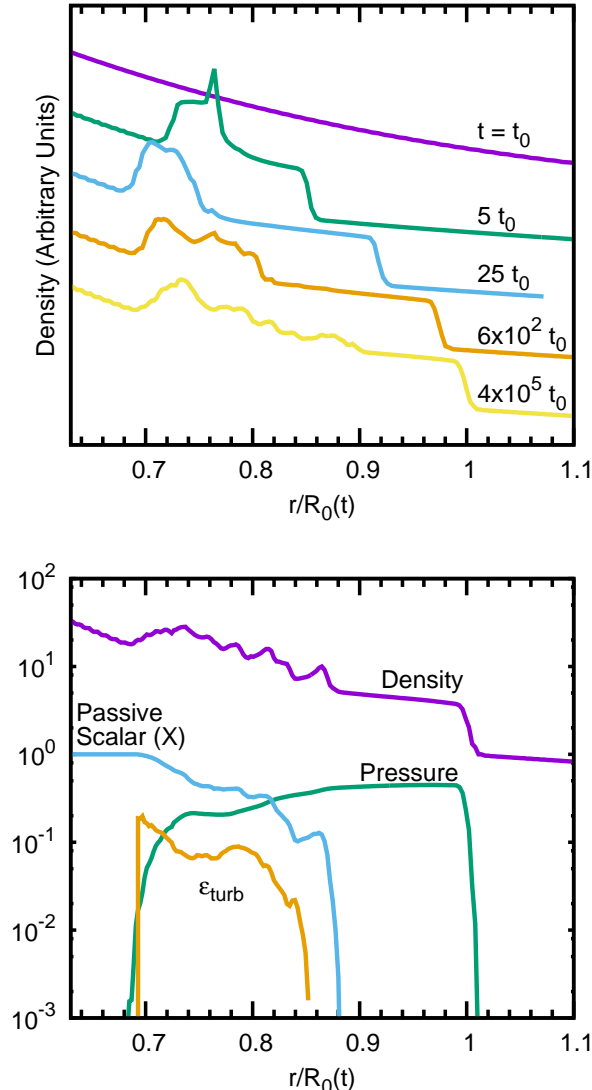


FIG. 2.— *Upper Panel:* Spherically-averaged profiles of density as a function of (re-scaled) radius at various times during the evolution. Density is plotted on an arbitrary scale, multiplied by an offset to facilitate comparison. After a time around $t \sim 100t_0$, the flow has attained a (statistically) self-similar state. *Lower Panel:* Profiles of density, pressure, X , and ϵ_{turb} in this self-similar solution. ϵ_{turb} attains values of order 0.1, but is concentrated near the reverse shock.

seed density fluctuations are $\delta_0 = 0.01$). The turbulence has grown to large scales, and (as Figure 2 shows) the coarse-grained properties of the flow are asymptoting toward a (statistically) self-similar solution. Note that this solution is distinct from the 1D self-similar solution of Chevalier, yet it still appears to obey the same scaling and self-similarity in the angle-averaged profile (scale invariance is not violated by allowing RT-induced mixing).

The top panel of Figure 2 shows the 1D averaged density, as it approaches statistical self-similarity, and the lower panel shows the late-time solution. Also shown in the lower panel is the quantity ϵ_{turb} , which takes on values as large as 10% and is concentrated in the mixed region just downstream of the reverse shock. Because turbulent mixing does not propagate all the way out to the forward shock, ϵ_{turb} falls to zero at larger radii. The

magnetic fields generated as a result of RT instabilities will therefore not uniformly fill the shocked region.

Most analyses of radio supernova observations have assumed a value of ϵ_B that is constant with radius. To compare to these studies, we define an “effective ϵ_B ” for our solutions that involves a weighted average of ϵ_{turb} over the shocked region. We begin with the synchrotron power radiated per unit volume between frequencies ν and $\nu + d\nu$

$$p_\nu d\nu = \frac{4}{3} \sigma_T c u_B \gamma^2 n(\gamma) d\gamma, \quad (15)$$

where σ_T is the Thompson cross-section, c is the speed of light, $u_B = B^2/8\pi$ is the magnetic energy density, and $n(\gamma)$ is the number density of non-thermal electrons as a function of their Lorentz factor γ . We assume that shock acceleration generates a standard power-law distribution, $n(\gamma) = C\gamma^{-p}$ for $\gamma > \gamma_{\text{min}}$. The constant $C = (p-1)n_{\text{nt}}\gamma_{\text{min}}^{p-1}$ where n_{nt} is the total number density of non-thermal electrons. In our study we take $p = 2.5$. Assuming that each electron radiates at its characteristic synchrotron frequency, $\nu_c = \gamma^2 eB/m_e c$, we can substitute into Eq. 15 and integrate over the shocked volume to get the specific luminosity

$$L_\nu = \int \frac{2}{3} C \sigma_T c u_B \nu_c^{-1} \left(\frac{\nu}{\nu_c} \right)^{(1-p)/2} 4\pi r^2 dr. \quad (16)$$

We assume that n_{nt} is a fixed fraction of the total gas density, $n_{\text{nt}} \propto \rho$, and that the energy density in non-thermal electrons is a fixed fraction of the total gas energy density, $u_{\text{nt}} \propto P$. Making the assumption $\epsilon_B \propto \epsilon_{\text{turb}}$, the integral can be expressed as

$$L_\nu = \text{const} \cdot \int \epsilon_{\text{turb}}^{(p+1)/4} F(r) dr, \quad (17)$$

where constants have pulled out of the integral, and $F(r)$ is defined as

$$F(r) = r^2 \rho (P/\rho)^{p-1} P^{(p+1)/4}. \quad (18)$$

The equivalent uniform ϵ_{turb} can now be calculated by an averaging process, weighting by $F(r)$

$$\langle \epsilon_{\text{turb}}(t) \rangle = \left(\frac{\int (\epsilon_{\text{turb}}(r))^{p+1} F(r) dr}{\int F(r) dr} \right)^{\frac{4}{p+1}} \quad (19)$$

The quantity $\langle \epsilon_{\text{turb}}(t) \rangle$ is an “effective average”, in the sense that it is equivalent to the ϵ_B that would be inferred if it were assumed that ϵ_B was uniform over the entire shocked region.

Figure 3 plots this averaged $\langle \epsilon_{\text{turb}} \rangle$ as a function of time for various choices of δ_0 . Regardless of the seed field, a common picture emerges: $\langle \epsilon_{\text{turb}} \rangle$ grows quickly, roughly as t^8 , until saturating around $\langle \epsilon_{\text{turb}} \rangle \sim 0.01$ after time $t \sim 100 t_0$. This growth appears to be independent of the magnitude of seed perturbations, so long as such perturbations are below order-unity.

The growth and saturated value of $\langle \epsilon_{\text{turb}} \rangle$ is largely independent of the seed field, and after time-averaging the saturation level is found to be $\langle \epsilon_{\text{turb}} \rangle \approx .0097$. Assuming magnetic fields are amplified to roughly 30–60% of this, we find $\epsilon_B \sim .003$ at a minimum due to RT alone.

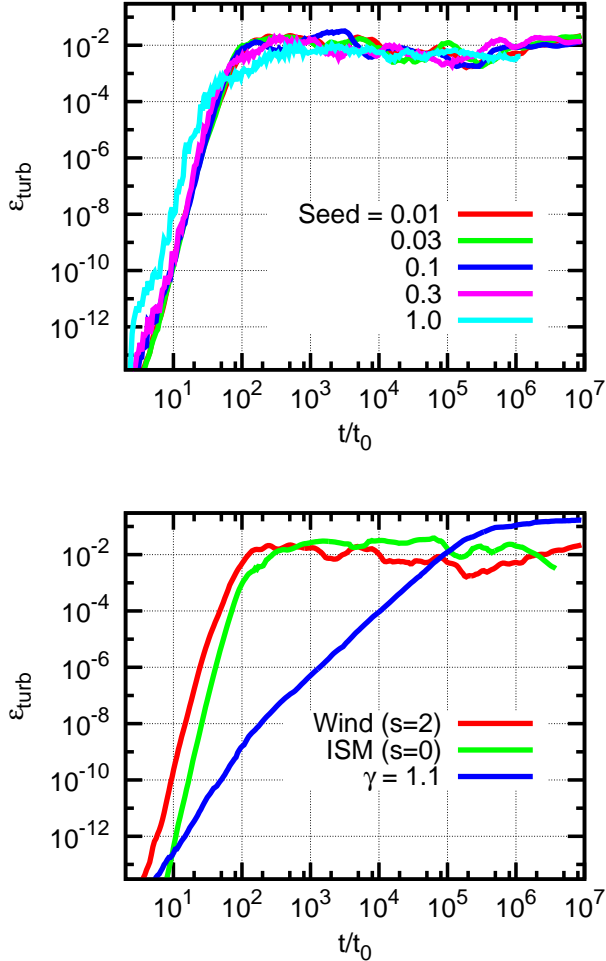


FIG. 3.— *Upper Panel:* Turbulent energy fraction (ϵ_{turb}) as a function of time for different magnitudes of seed perturbation. The turbulence is nearly independent of seed field, except for the case of order-unity perturbations $\delta_0 = 1.0$. For all cases, turbulent fluctuations grow as $\sim t^8$, and saturation is established around $t \sim 100 t_0$. The turbulent energy fraction finds a final saturated state at $\epsilon_{\text{turb}} \sim 0.01$. *Lower Panel:* Solution is tested for different hydrodynamical models. Choosing a uniform CSM (“ISM Model”) results in a very similar progression for the turbulent amplification. Reducing the adiabatic index results in a much larger saturation value of $\epsilon_{\text{turb}} \sim 0.3$, but saturation occurs much later, around $t \sim 10^5 t_0$. This suggests that cosmic ray cooling could affect these results, potentially enhancing ϵ_B , but also affecting the timescale for saturation.

Results are also included in Figure 3 for an additional “ISM” model, where the CSM density is uniform ($s = 0$, lower panel). This resulted in very similar behavior, suggesting that the strength of the turbulence is not sensitive to the detailed initial setup.

As a first attempt at modeling the effects of cooling, we perform an additional calculation with a soft equation of state, using an adiabatic index $\gamma = 1.1$, rather than the $\gamma = 5/3$ value used primarily in this study. In the lower panel of Figure 3, $\epsilon_{\text{turb}}(t)$ is shown for the $\gamma = 1.1$ calculation, showing that softening the equation of state impacts the results. Because the shocked region is narrower for lower γ , turbulence catches up to the forward shock (as noticed by Blondin & Ellison (2001)). Nearly the entire shocked region becomes turbulent and magnetized,

increasing the emitting volume and therefore the “effective average” of ϵ_{turb} . We find saturation at $\epsilon_{\text{turb}} \sim 0.3$, suggesting a floor of $\epsilon_B \sim 0.1$. However, the timescale for reaching saturation is also affected by the equation of state, causing saturation as late as $10^5 t_0$. A more detailed calculation including realistic models for cooling is warranted, and will be attempted in a future study.

4. DISCUSSION

RT instability generates turbulence in interacting supernovae, which is amplified until reaching a saturated state after time $t \sim 100 t_0$, where t_0 is the time when the encounter with the ambient medium begins: $t_0 \sim R_0/v_0$, where R_0 is the inner radius of the CSM and v_0 is the ejecta velocity. This timescale for saturation is in agreement with that found by Chevalier et al. (1992). For example, assuming observed ejecta velocities of $v_0 \sim 10^9$ cm/sec, and a CSM around a solar-size progenitor, $R_0 \sim 10^{11}$ cm, the saturated turbulent state is reached after $100 t_0 \sim$ hours. For CSM around a larger progenitor (such as a red supergiant), $100 t_0 \sim$ days, while for a more compact progenitor (as a white dwarf in a type-Ia supernovae) $100 t_0 \sim$ minutes. These numbers are independent of the clumpiness of the surrounding medium, so long as such clumpiness consists of less than order-unity perturbations to the density.

If RT generated turbulence is the only mechanism producing magnetic fields in interacting supernovae, then one would expect to see significantly less emission prior to $t \sim 100 t_0$. Depending on the distribution of CSM, this may have a significant impact on the predicted light curves of radio supernovae. The initial stages of the interaction may be rendered radio invisible, as the magnetic fields have not had time to be amplified.

Assuming magnetic energy is amplified to equipartition with kinetic fluctuations, the saturated magnetic field in the asymptotic state is $\epsilon_B \sim 3\%$ of equipartition with the thermal energy in the vicinity of the reverse shock. If no other mechanism produces sufficient magnetic fields, the reverse shock dominates the synchrotron emission, which is in contrast to standard models assuming a constant ϵ_B , where the reverse shock contributes only $\sim 10\%$ of the total luminosity. A value of $\epsilon_B \sim 3\%$ near the reverse shock translates to an effective averaged magnetic energy of $\epsilon_B \sim 0.3\%$; that is, it generates as much synchrotron flux as a supernova with uniform $\epsilon_B \sim 3 \times 10^{-3}$ everywhere. Therefore, applying the value $\epsilon_B \sim 3 \times 10^{-3}$ is justified in that it is a lower bound to the magnetic field strength which should be present in all supernovae from Rayleigh-Taylor instability alone.

These numbers may be enhanced by cosmic ray cooling, as it has a significant impact on the dynamics of RT (Blondin & Ellison 2001). Cosmic rays provide significant cooling in shocks, slowing down the forward shock, and reducing the steepness of pressure gradients, allowing the Rayleigh-Taylor fingers to propagate through the entire shocked region. This was demonstrated first by Blondin & Ellison (2001), by varying the adiabatic index, as an effective proxy for cooling. This has also been shown in the relativistic case (Duffell & MacFadyen 2014). Fraschetti et al. (2010) and Ferrand et al. (2010) have also seen this effect, using a prescribed model for cosmic ray cooling (rather than varying the adiabatic index). The importance of cosmic rays on the dynam-

ics has also been shown observationally (Warren et al. 2005). Our studies using a softer equation of state demonstrate this trend, suggesting that the floor on ϵ_B is even larger than the conservative 0.3% minimum calcu-

lated here (though it appears the softer equation of state affects the timescale for saturation, see Figure 3). A full calculation including these effects (and the effects of 3D turbulence) will be attempted in a future study.

REFERENCES

- Beresnyak, A. 2012, *Physical Review Letters*, 108, 035002
 Blondin, J. M., & Ellison, D. C. 2001, *ApJ*, 560, 244
 Chevalier, R. A. 1982, *ApJ*, 258, 790
 Chevalier, R. A., Blondin, J. M., & Emmering, R. T. 1992, *ApJ*, 392, 118
 Chevalier, R. A., & Fransson, C. 2006, *ApJ*, 651, 381
 Chomiuk, L., Soderberg, A. M., Moe, M., et al. 2012, *ApJ*, 750, 164
 Chomiuk, L., Soderberg, A. M., Chevalier, R. A., et al. 2015, *ArXiv e-prints*, arXiv:1510.07662
 Duffell, P. C., & MacFadyen, A. I. 2011, *ApJS*, 197, 15
 —. 2013, *ApJ*, 775, 87
 —. 2014, *ApJ*, 791, L1
 Ferrand, G., Decourchelle, A., Ballet, J., Teyssier, R., & Fraschetti, F. 2010, *A&A*, 509, L10
 Fraschetti, F., Teyssier, R., Ballet, J., & Decourchelle, A. 2010, *A&A*, 515, A104
 Giacomazzo, B., Zrake, J., Duffell, P. C., MacFadyen, A. I., & Perna, R. 2015, *ApJ*, 809, 39
 Gruzinov, A., & Waxman, E. 1999, *ApJ*, 511, 852
 Haugen, N. E. L., Brandenburg, A., & Dobler, W. 2003, *ApJ*, 597, L141
 Horesh, A., Kulkarni, S. R., Fox, D. B., et al. 2012, *ApJ*, 746, 21
 Jun, B.-I., & Norman, M. L. 1996, *ApJ*, 465, 800
 Jun, B.-I., Norman, M. L., & Stone, J. M. 1995, *ApJ*, 453, 332
 Kane, J., Arnett, D., Remington, B. A., et al. 2000, *ApJ*, 528, 989
 Kazantsev, A. 1968, *Sov. Phys. JETP*, 26, 1031
 Kiuchi, K., Cerdá-Durán, P., Kyutoku, K., Sekiguchi, Y., & Shibata, M. 2015, *ArXiv e-prints*, arXiv:1509.09205
 Medvedev, M. V., & Loeb, A. 1999, *ApJ*, 526, 697
 Moffatt, H. K. 1978, *Magnetic field generation in electrically conducting fluids*
 Nishikawa, K.-I., Hardee, P., Richardson, G., et al. 2003, *ApJ*, 595, 555
 Patat, F., Chandra, P., Chevalier, R., et al. 2007, *Science*, 317, 924
 Schekochihin, A. A., Cowley, S. C., Taylor, S. F., Maron, J. L., & McWilliams, J. C. 2004, *ApJ*, 612, 276
 Soderberg, A. M., Margutti, R., Zauderer, B. A., et al. 2012, *ApJ*, 752, 78
 Spitkovsky, A. 2008, *ApJ*, 682, L5
 Warren, J. S., Hughes, J. P., & Badenes, C. 2005, in *Bulletin of the American Astronomical Society*, Vol. 37, American Astronomical Society Meeting Abstracts, 172.12
 Zrake, J., & MacFadyen, A. I. 2013, *ApJ*, 769, L29